Biomedical Optics EXPRESS

Quantitative assessment of graded burn wounds in a porcine model using spatial frequency domain imaging (SFDI) and laser speckle imaging (LSI)

Adrien Ponticorvo,[1,4] David M. Burmeister,[3,4] Bruce Yang,[1] Bernard Choi,[1,2] Robert J. Christy,[3] and Anthony J. Durkin[1,*]

[1]*Beckman Laser Institute and Medical Clinic, University of California, Irvine, 1002 Health Sciences Road East, Irvine, CA 92617, USA*

[2]*Department of Biomedical Engineering, University of California, Irvine, 3120 Natural Sciences II, Irvine, CA 92697, USA*

[3]*United States Army Institute of Surgical Research, 3698 Chambers Pass, Fort Sam Houston, TX, 78234, USA*

[4]*co-first authors*

**adurkin@uci.edu*

Abstract: Accurate and timely assessment of burn wound severity is a critical component of wound management and has implications related to course of treatment. While most superficial burns and full thickness burns are easily diagnosed through visual inspection, burns that fall between these extremes are challenging to classify based on clinical appearance. Because of this, appropriate burn management may be delayed, increasing the risk of scarring and infection. Here we present an investigation that employs spatial frequency domain imaging (SFDI) and laser speckle imaging (LSI) as non-invasive technologies to characterize *in-vivo* burn severity. We used SFDI and LSI to investigate controlled burn wounds of graded severity in a Yorkshire pig model. Burn wounds were imaged starting at one hour after the initial injury and daily at approximately 24, 48 and 72 hours post burn. Biopsies were taken on each day in order to correlate the imaging data to the extent of burn damage as indicated via histological analysis. Changes in reduced scattering coefficient and blood flow could be used to categorize burn severity as soon as one hour after the burn injury. The results of this study suggest that SFDI and LSI information have the potential to provide useful metrics for quantifying the extent and severity of burn injuries.

OCIS codes: (110.4234) Multispectral and hyperspectral imaging; (170.3660) Light propagation in tissues; (170.3880) Medical optics and biotechnology; (170.6510) Spectroscopy, tissue diagnostics.

References and links

1. C. E. White and E. M. Renz, "Advances in surgical care: management of severe burn injury," Crit. Care Med. **36**(7 Suppl), S318–S324 (2008).
2. L. Devgan, S. Bhat, S. Aylward, and R. J. Spence, "Modalities for the assessment of burn wound depth," J. Burns Wounds **5**, e2 (2006).
3. D. J. McGill, K. Sørensen, I. R. MacKay, I. Taggart, and S. B. Watson, "Assessment of burn depth: a prospective, blinded comparison of laser Doppler imaging and videomicroscopy," Burns **33**(7), 833–842 (2007).
4. A. M. Watts, M. P. Tyler, M. E. Perry, A. H. Roberts, and D. A. McGrouther, "Burn depth and its histological measurement," Burns **27**(2), 154–160 (2001).
5. H. Hoeksema, K. Van De Sijpe, T. Tondu, M. Hamdi, K. Van Landuyt, P. Blondeel, and S. Monstrey, "Accuracy of early burn depth assessment by laser Doppler imaging on different days post burn," Burns **35**(1), 36–45 (2009).

#217716 - $15.00 USD Received 24 Jul 2014; accepted 28 Aug 2014; published 8 Sep 2014

6. S. C. Davis, P. M. Mertz, E. D. Bilevich, A. L. Cazzaniga, and W. H. Eaglstein, "Early debridement of second-degree burn wounds enhances the rate of epithelization--an animal model to evaluate burn wound therapies," J. Burn Care Rehabil. **17**(6), 558–561 (1996).
7. M. Eski, F. Ozer, C. Firat, D. Alhan, N. Arslan, T. Senturk, and S. Işik, "Cerium nitrate treatment prevents progressive tissue necrosis in the zone of stasis following burn," Burns **38**(2), 283–289 (2012).
8. C. Firat, E. Samdanci, S. Erbatur, A. H. Aytekin, M. Ak, M. G. Turtay, and Y. K. Coban, "β-Glucan treatment prevents progressive burn ischaemia in the zone of stasis and improves burn healing: An experimental study in rats," Burns **39**(1), 105–112 (2013).
9. M. Nisanci, M. Eski, I. Sahin, S. Ilgan, and S. Isik, "Saving the zone of stasis in burns with activated protein C: an experimental study in rats," Burns **36**(3), 397–402 (2010).
10. M. Kaiser, A. Yafi, M. Cinat, B. Choi, and A. J. Durkin, "Noninvasive assessment of burn wound severity using optical technology: a review of current and future modalities," Burns **37**(3), 377–386 (2011).
11. S. A. Pape, C. A. Skouras, and P. O. Byrne, "An audit of the use of laser Doppler imaging (LDI) in the assessment of burns of intermediate depth," Burns **27**(3), 233–239 (2001).
12. M. H. Arbab, T. C. Dickey, D. P. Winebrenner, A. Chen, M. B. Klein, and P. D. Mourad, "Terahertz reflectometry of burn wounds in a rat model," Biomed. Opt. Express **2**(8), 2339–2347 (2011).
13. J. Y. Suen, P. Tewari, Z. D. Taylor, W. S. Grundfest, H. Lee, E. R. Brown, M. O. Culjat, and R. S. Singh, "Towards medical terahertz sensing of skin hydration," Stud. Health Technol. Inform. **142**, 364–368 (2009).
14. K. Aizawa, S. Sato, D. Saitoh, H. Ashida, and M. Obara, "Photoacoustic monitoring of burn healing process in rats," J. Biomed. Opt. **13**(6), 064020 (2008).
15. H. F. Zhang, K. Maslov, G. Stoica, and L. V. Wang, "Imaging acute thermal burns by photoacoustic microscopy," J. Biomed. Opt. **11**(5), 054033 (2006).
16. K. M. Cross, L. Leonardi, M. Gomez, J. R. Freisen, M. A. Levasseur, B. J. Schattka, M. G. Sowa, and J. S. Fish, "Noninvasive measurement of edema in partial thickness burn wounds," J. Burn Care Res. **30**(5), 807–817 (2009).
17. K. M. Cross, L. Leonardi, J. R. Payette, M. Gomez, M. A. Levasseur, B. J. Schattka, M. G. Sowa, and J. S. Fish, "Clinical utilization of near-infrared spectroscopy devices for burn depth assessment," Wound Repair Regen. **15**(3), 332–340 (2007).
18. M. G. Sowa, L. Leonardi, J. R. Payette, K. M. Cross, M. Gomez, and J. S. Fish, "Classification of burn injuries using near-infrared spectroscopy," J. Biomed. Opt. **11**(5), 054002 (2006).
19. M. G. Sowa, L. Leonardi, J. R. Payette, J. S. Fish, and H. H. Mantsch, "Near infrared spectroscopic assessment of hemodynamic changes in the early post-burn period," Burns **27**(3), 241–249 (2001).
20. D. Yudovsky, A. Nouvong, K. Schomacker, and L. Pilon, "Assessing diabetic foot ulcer development risk with hyperspectral tissue oximetry," J. Biomed. Opt. **16**(2), 026009 (2011).
21. A. J. Durkin, J. G. Kim, and D. J. Cuccia, "Quantitative Near Infrared Imaging of Skin Flaps," in *BioMed 2008*, (American Society of Mechanical Engineers, 2008).
22. S. Gioux, A. Mazhar, D. J. Cuccia, A. J. Durkin, B. J. Tromberg, and J. V. Frangioni, "Spatially-modulated near-infrared imaging for image-guided surgery," in *World Molecular Imaging Congress*, (World Molecular Imaging Society, 2008).
23. S. D. Konecky, A. Mazhar, D. Cuccia, A. J. Durkin, J. C. Schotland, and B. J. Tromberg, "Quantitative optical tomography of sub-surface heterogeneities using spatially modulated structured light," Opt. Express **17**(17), 14780–14790 (2009).
24. A. Mazhar, S. A. Sharif, J. D. Cuccia, J. S. Nelson, K. M. Kelly, and A. J. Durkin, "Spatial frequency domain imaging of port wine stain biochemical composition in response to laser therapy: A pilot study," Lasers Surg. Med. **44**(8), 611–621 (2012).
25. M. R. Pharaon, T. Scholz, S. Bogdanoff, D. Cuccia, A. J. Durkin, D. B. Hoyt, and G. R. Evans, "Early detection of complete vascular occlusion in a pedicle flap model using quantitative [corrected] spectral imaging," Plast. Reconstr. Surg. **126**(6), 1924–1935 (2010).
26. A. Yafi, T. S. Vetter, T. Scholz, S. Patel, R. B. Saager, D. J. Cuccia, G. R. Evans, and A. J. Durkin, "Postoperative quantitative assessment of reconstructive tissue status in a cutaneous flap model using spatial frequency domain imaging," Plast. Reconstr. Surg. **127**(1), 117–130 (2011).
27. J. Nguyen, C. Crouzet, T. Mai, K. Riola, D. Uchitel, L. Liaw, N. Bernal, A. Ponticorvo, B. Choi, and A. Durkin, "Quantitative Longitudinal Measurement in a Rat Model of Controlled Burn Severity Using Spatial Frequency Domain Imaging " in *Photonics West*, (SPIE, 2013).
28. J. Q. Nguyen, C. Crouzet, T. Mai, K. Riola, D. Uchitel, L. H. Liaw, N. Bernal, A. Ponticorvo, B. Choi, and A. J. Durkin, "Spatial frequency domain imaging of burn wounds in a preclinical model of graded burn severity," J. Biomed. Opt. **18**(6), 066010 (2013).
29. C. Gaines, D. Poranki, W. Du, R. A. Clark, and M. Van Dyke, "Development of a porcine deep partial thickness burn model," Burns **39**(2), 311–319 (2013).
30. A. Ponticorvo, E. Taydas, A. Mazhar, T. Scholz, H. S. Kim, J. Rimler, G. R. Evans, D. J. Cuccia, and A. J. Durkin, "Quantitative assessment of partial vascular occlusions in a swine pedicle flap model using spatial frequency domain imaging," Biomed. Opt. Express **4**(2), 298–306 (2013).
31. D. J. Cuccia, F. Bevilacqua, A. J. Durkin, F. R. Ayers, and B. J. Tromberg, "Quantitation and mapping of tissue optical properties using modulated imaging," J. Biomed. Opt. **14**(2), 024012 (2009).

#217716 - $15.00 USD Received 24 Jul 2014; accepted 28 Aug 2014; published 8 Sep 2014

32. A. Mazhar, S. Dell, D. J. Cuccia, S. Gioux, A. J. Durkin, J. V. Frangioni, and B. J. Tromberg, "Wavelength optimization for rapid chromophore mapping using spatial frequency domain imaging," J. Biomed. Opt. **15**(6), 061716 (2010).
33. T. A. Erickson, A. Mazhar, D. Cuccia, A. J. Durkin, and J. W. Tunnell, "Lookup-table method for imaging optical properties with structured illumination beyond the diffusion theory regime," J. Biomed. Opt. **15**(3), 036013 (2010).
34. S. Gioux, A. Mazhar, D. J. Cuccia, A. J. Durkin, B. J. Tromberg, and J. V. Frangioni, "Three-dimensional surface profile intensity correction for spatially modulated imaging," J. Biomed. Opt. **14**(3), 034045 (2009).
35. O. Yang, D. Cuccia, and B. Choi, "Real-time blood flow visualization using the graphics processing unit," J. Biomed. Opt. **16**(1), 016009 (2011).
36. G. Aguilar, B. Choi, M. Broekgaarden, O. Yang, B. Yang, P. Ghasri, J. K. Chen, R. Bezemer, J. S. Nelson, A. M. Van Drooge, A. Wolkerstorfer, K. M. Kelly, and M. Heger, "An overview of three promising mechanical, optical, and biochemical engineering approaches to improve selective photothermolysis of refractory port wine stains," Ann. Biomed. Eng. **40**(2), 486–506 (2012).
37. J. W. Shupp, T. J. Nasabzadeh, D. S. Rosenthal, M. H. Jordan, P. Fidler, and J. C. Jeng, "A review of the local pathophysiologic bases of burn wound progression," J. Burn Care Res. **31**(6), 849–873 (2010).
38. D. Heimbach, L. Engrav, B. Grube, and J. Marvin, "Burn depth: a review," World J. Surg. **16**(1), 10–15 (1992).
39. M. Chvapil, D. P. Speer, J. A. Owen, and T. A. Chvapil, "Identification of the depth of burn injury by collagen stainability," Plast. Reconstr. Surg. **73**(3), 438–441 (1984).
40. S. Thomsen, "Pathologic analysis of photothermal and photomechanical effects of laser-tissue interactions," Photochem. Photobiol. **53**(6), 825–835 (1991).
41. M. Kempf, L. Cuttle, P. Y. Liu, X. Q. Wang, and R. M. Kimble, "Important improvements to porcine skin burn models, in search of the perfect burn," Burns **35**(3), 454–455 (2009).
42. A. Papp, K. Kiraly, M. Härmä, T. Lahtinen, A. Uusaro, and E. Alhava, "The progression of burn depth in experimental burns: a histological and methodological study," Burns **30**(7), 684–690 (2004).
43. A. J. Singer and S. A. McClain, "A porcine burn model," Methods Mol. Med. **78**, 107–119 (2003).
44. A. D. Jaskille, J. C. Ramella-Roman, J. W. Shupp, M. H. Jordan, and J. C. Jeng, "Critical review of burn depth assessment techniques: part II. Review of laser doppler technology," J. Burn Care Res. **31**(1), 151–157 (2010).
45. P. Ganapathy, T. Tamminedi, Y. Qin, L. Nanney, N. Cardwell, A. Pollins, K. Sexton, and J. Yadegar, "Dual-imaging system for burn depth diagnosis," Burns **40**(1), 67–81 (2014).

1. Introduction

In the United States, 500,000 people annually seek out treatment for burns and almost 10% of that group will require hospitalization [1]. One of the most challenging and critical aspects for clinicians treating burn wounds is accurately diagnosing burn severity. This is because the treatment plan for a patient is directly related to the initial diagnosis. Superficial (first-degree) burns are minor and will generally heal on their own, but full thickness (third-degree) burns that destroy the thickness of the dermis and parts of the underlying hypodermis require surgical intervention. While superficial and full-thickness burns types are relatively straightforward for clinicians to diagnose based on appearance, it is more difficult to categorize partial thickness burns (second-degree) that can fall in between the superficial or deep category. The accuracy of diagnosing these partial thickness burns by clinicians is typically 60-80% when the diagnosis is done several days after the burn injury [2–4]. However, when clinicians attempt to make the diagnosis within the first 24-48 hours of the occurrence of a burn, the accuracy of the diagnosis decreases to 50% [5]. This is largely due to the dynamic nature of burn wounds during the first 48 hours. This is also the reason that clinical assessments are typically made several days after the initial burn [2] even though earlier intervention has been shown to improve healing [6], reduce complication rates (infection, scarring) and shorten hospital stays for patients [7–9]. This highlights the rationale for developing new objective techniques that will enable more timely decision making related to burn wound severity and management.

Efforts to improve upon the objectivity of burn severity assessment have focused on the use of technologies to observe blood flow, the patency of the microvasculature, and overall tissue damage and include methods such as thermography, vital dyes, indocyanine green video angiography and laser Doppler techniques [2]. Recently we have reviewed technologies that have been employed to assess burn severity [10]. Of these technologies, Laser Doppler Imaging (LDI) appears to offer the best data-supported estimates of burn severity [2, 5, 11]. LDI allows a clinician to visualize the spatial variation of perfusion, a key indicator of burn

#217716 - $15.00 USD Received 24 Jul 2014; accepted 28 Aug 2014; published 8 Sep 2014

depths and eventual healing times. One of the issues associated with LDI, however, is that the analysis often measures relatively superficial blood flow, when quantitative, deeper analysis would be more informative to burn management, particularly with respect to differentiating superficial partial thickness burns from deep partial thickness burns [2, 3]. In addition, for many of the LDI systems that are currently available, the laser is mechanically scanned over the patient for up to 5 minutes per image, resulting in movement artifacts and long data collection times for large surface area burns [3]. The detection of blood flow alone does not provide the definitive information regarding tissue health, particularly in the case of partial-thickness burns [2, 3]. LDI is less accurate when utilized within the first 24-48 hours of injury [5, 11] and healing studies indicate that it is not until post-burn day 3 that severity assessment using LDI becomes significantly better than clinical assessment [5].

Recently, feasibility studies using terahertz (THz) imaging have been carried out with the objective of gauging its potential as a burn severity assessment tool [12]. Reflective THz imaging relies on the dielectric properties of water to reflect the signal of interrogated tissue. Electromagnetic waves in the 1 mm – 0.1 mm (300 GHz – 3 THz) regime are generated by a femtosecond pulse laser and raster-scanned over a region of tissue. The variance in the measured reflectance is proportional to the local water content [13]. Thus, edema response in burn tissue has become a key research area in biological tissue. Unfortunately, the signal is affected by surface irregularities, scan times are slow and the instrument cost (> $100,000) is generally prohibitive in its current state of development. This approach also does not provide information related to hemodynamics. Photoacoustic microscopy (PAM) is another technology that is being investigated by various groups to image burn wounds [14, 15]. In experimental models of burns, PAM was able to distinguish different durations of thermal exposure within minutes of injury. While this research appears to be promising, PAM approaches are limited to a relatively small field of view (mm) which limits practicality in terms of canvassing large areas of burn tissue, as they are often highly heterogeneous in terms of burn severity.

Finally, both traditional diffuse reflectance spectroscopy (DRS) and imaging have been investigated within the context of burn wounds by various groups [16–19]. Visible and near infrared (NIR) polarized light is used to illuminate the tissue and the remitted cross-polarized light is captured with a camera or fiber to isolate subsurface features in tissue. Primary contrast mechanisms in tissue are oxygenated and deoxygenated hemoglobin in the visible wavelength regime and the same plus water in the NIR. DRS at visible wavelengths has a limited penetration depth and is suited to assessment of superficial wounds [20]. NIR light has the benefit of enabling imaging several millimeters deep in tissue and has been applied to pre-clinical burn measurements [16, 19]. However, in the absence of an appropriate accounting system that can separate and resolve changes that result from absorption and scattering, these techniques can suffer from inaccurate results that have limited the progression of the technology in the clinic.

Spatial frequency domain imaging (SFDI) is a unique, wide-field imaging modality that has been invented, and developed at the Beckman Laser Institute (BLI). It is based on diffuse optical spectroscopic principles and is well-suited for quantitative imaging of tissue [21–28]. This non-contact, *in-vivo* technique provides quantitative, spatial maps of tissue optical properties and biochemical composition for fields of view over 100 cm^2. SFDI is potentially able to quantitatively capture information related to collagen denaturation (via scattering changes), hemodynamics and vascular damage each of which have the potential to provide clinicians with objective means to assess burn wound severity.

Laser speckle imaging (LSI) is a noninvasive technique based on the analysis of fluctuations in a speckle pattern to quantify motion such as blood flow. While LDI and LSI essentially measure the same physiological phenomenon, LSI has the ability to image an entire field of view at a single time point and in real-time as opposed to LDI which must take time to scan over a similar region. As such, LSI has the potential to avoid artifacts associated

#217716 - $15.00 USD Received 24 Jul 2014; accepted 28 Aug 2014; published 8 Sep 2014

with movements or small hemodynamic fluctuations to assess changes in blood flow that could be associated with varying burn severity.

If the structural and functional information quantified by SFDI and LSI can provide diagnostically compelling information at earlier time points than visual inspection and LDI, this would suggest the potential for shorter hospital stays for patients and improved wound healing [6]. While earlier studies examining these imaging technologies in rat burns have been promising [28], porcine skin is a much closer surrogate to human skin [29]. In order to further investigate how the physiological parameters measured by SFDI and LSI could noninvasively characterize burn severity, we examined the performance of these techniques in a controlled swine burn model. Burn wounds of graded severity ranging from superficial partial thickness burns to full thickness burns were created on the dorsum of a pig, and burn extent was verified histologically. We examined these burn wounds with SFDI and LSI at 1 hour post burn, and then again every subsequent day, at approximately 24, 48 and 72 hours post-burn.

2. Methodology

2.1 Spatial frequency domain imaging (SFDI)

The setup for the SFDI instrumentation has been described in detail before [30, 31], and a brief description is provided below. A prototype clinical imaging system (v100, Modulated Imaging Inc., Irvine, CA) was used to acquire the burn data. The instrument consisted of a near-infrared camera with cross-polarizers to reduce specular reflection. A light source with LEDs centered at 658, 730, and 850 nm [32] was projected off of a spatial light modulator, Digital Micromirror Device (DMD Discovery 1100, Texas Instruments Inc., Dallas, TX). These devices were housed in a compact cubic enclosure (~1 ft^3) that was mounted on an articulating arm attached to a portable cart. The field of view was approximately 13.5 cm x 10.5 cm. A sinusoidal pattern of 0.2 mm^{-1} frequency was projected onto the sample at three phases (0, 120, and 240 degrees) by each of the LEDs in addition to uniform DC illumination (0 mm^{-1}) and a profilometry measurement. It took approximately 12 seconds to collect one sequence of data, and this process was repeated every 30 seconds. Custom C# software (Modulated Imaging Inc., Irvine, CA) was used to control the hardware.

We have described the procedure for determining absorption and reduced scattering coefficients in previous publications [28, 30, 31]. Briefly, MATLAB (Natick, MA) was used to analyze the collected image data. The demodulation of the three phase images was used to determine the AC component while the DC component was determined from the uniform illumination images. This data was then used to estimate the absorption and reduced scattering coefficient properties based on a lookup table. Using an analysis approach similar to what we have employed in previously reported SFDI based research [30], a single white Monte Carlo simulation was generated and then scaled to determine lookup table values for different optical properties [33]. A surface profilometry calibration measurement of a sample with known optical properties was used to correct the effects of surface curvature and day to day instrument variations [34]. The absorption maps at each wavelength were used to estimate chromophore concentration maps of oxygenated and deoxygenated hemoglobin that could be converted to tissue oxygen saturation (stO_2) by dividing oxygenated hemoglobin by the sum of oxygenated and deoxygenated hemoglobin. Maps of the reduced scattering coefficient at each of the wavelengths were also generated using this technique.

2.2 Laser speckle imaging (LSI)

The LSI instrument consisted of three main hardware components: a laser source, CCD camera, and computer. The laser source was a continuous-wave HeNe laser light (λ = 633 nm, 30 mW, Edmund Industrial Optics, Barrington, NJ). The CCD camera was a thermoelectrically-cooled Retiga 2000R (QImaging, Burnaby, BC, Canada) with a pixel

#217716 - $15.00 USD Received 24 Jul 2014; accepted 28 Aug 2014; published 8 Sep 2014

resolution of 1600 x 1200 (1.92 megapixels, each pixel having dimensions of 7.4 µm x 7.4 µm). The laptop (Sager P170EM, City of Industry, CA) was equipped with a GTX650 Graphics Processing Unit (GPU) (NVIDIA, Santa Clara, CA). A laser speckle pattern was generated by the 633nm laser source and projected onto the region of interest. This raw laser speckle image was then recorded with the CCD camera and processed on the computer using custom LabVIEW (Version 8.0, National Instruments, Austin, TX) software, integrating CUDA GPU code to carry out real-time LSI imaging and processing at a rate of eight frames per second [35, 36]. The processed speckle image provides a blood flow map for the region of interest. Blood flow is quantified by a metric known as Speckle Flow Index (SFI), which we have described previously [36]. Regions in which SFI values are high correspond to high blood flow and regions in which SFI values are low indicated areas of low blood flow. Data was collected sequentially for every burn wound using the LSI and SFDI instruments. A schematic of illustrating the data collection geometry using devices is shown in Fig. 1 below.

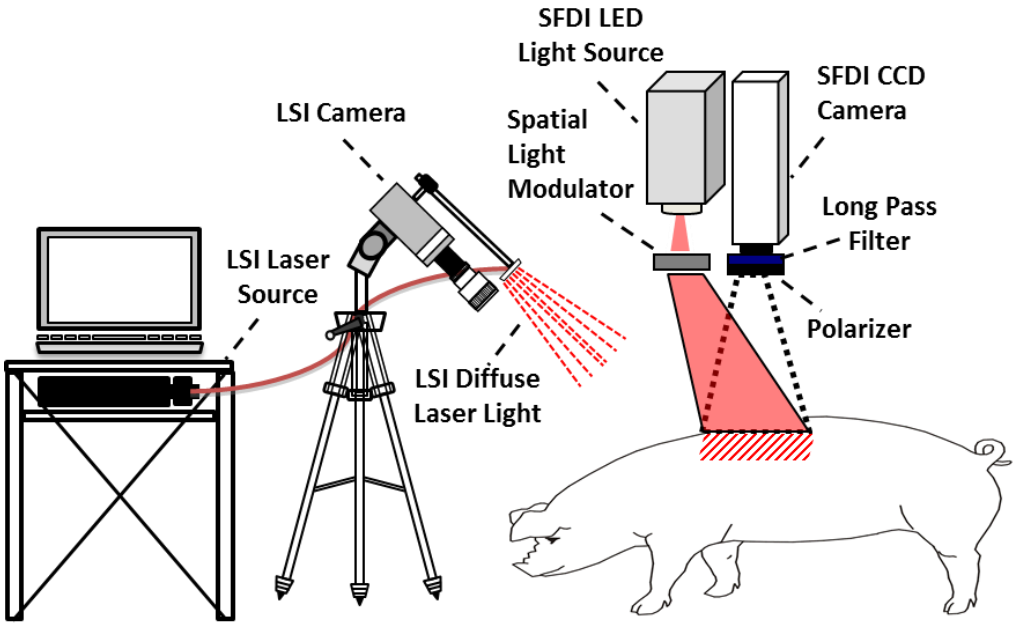

Fig. 1. Diagram illustrating the data collection geometry used in the experiment.

2.3 Animals

All experiments were performed in accordance with the United States Army Institute of Surgical Research Animal Care Use Committee (protocol #A-13-018). Two Yorkshire pigs (49.5 kg average weight) were used in this experiment. Animals were individually housed, had access to water, and acclimated to the facilities for at least 7 days prior to use. Animals were fasted the day before anesthesia, at which time a transdermal fentanyl patch (100µg/hr) was placed on the ear.

Prior to anesthesia for the burn procedure and debridement (days 0 and 4 respectively), the pig was premedicated with glycopyrrolate (0.01mg/kg, IM) to minimize salivation and bradycardia during the surgical procedure. Anesthesia was induced with an intramuscular injection of tiletamine-zolazepam (Telazol, 6 mg/kg). Animals were then intubated with an endotracheal tube and placed on an automatic ventilator with the initial tidal volume at 10 ml/kg, peak pressure at 20 cmH_2O and respiration rate at 8 to 12 breaths per minute. The ventilator setting was adjusted to maintain an end tidal PCO_2 of 40 ± 5 mmHg, and anesthesia was maintained with 1% to 3% isofluorane (balance oxygen). Vital signs were continuously

#217716 - $15.00 USD Received 24 Jul 2014; accepted 28 Aug 2014; published 8 Sep 2014

monitored and kept constant by adjusting anesthesia levels. A heating blanket was used to maintain a constant body temperature (36-38°C).

2.4 Creation of controlled, graded burn wounds

Controlled, graded burn wounds were created using a custom-made device setup described previously [29]. Briefly, cylindrical brass probes (3 cm diameter) with stainless steel posts were fabricated to fit into a spring loaded Teflon insulated device to ensure a consistent, reproducible pressure when applied to the skin (Fig. 2(a)). The brass probes were placed in a hard-anodized aluminum block, and heated in a warm bath incubator to 100°C. Hair was removed from the dorsum of the swine with clippers, and the back was sterilized with chlorohexidine. A 3 cm circular tracing template was used to mark areas for burn wound placement. These were located 1.5 cm from the spine and 2.5 cm away from each other (Fig. 2(a)) in order to allow enough space so that each wound would be independent and free of competing healing responses from adjacent burn areas [29]. In all, 16 wounds were created on either side of the spine, with contact times of 5, 10, 15, 20, 25, 30, 35, and 40 seconds (Fig. 2(b)). Wounds (n = 4 per contact time) were dressed with a non-adherent gauze (Telfa, Tyco Healthcare, Mansfield, MA) along with antibiotic Ioban (3M, St. Paul, MN), all held in place with Elastikon surgical tape (Johnson and Johnson, New Brunswick, NJ).

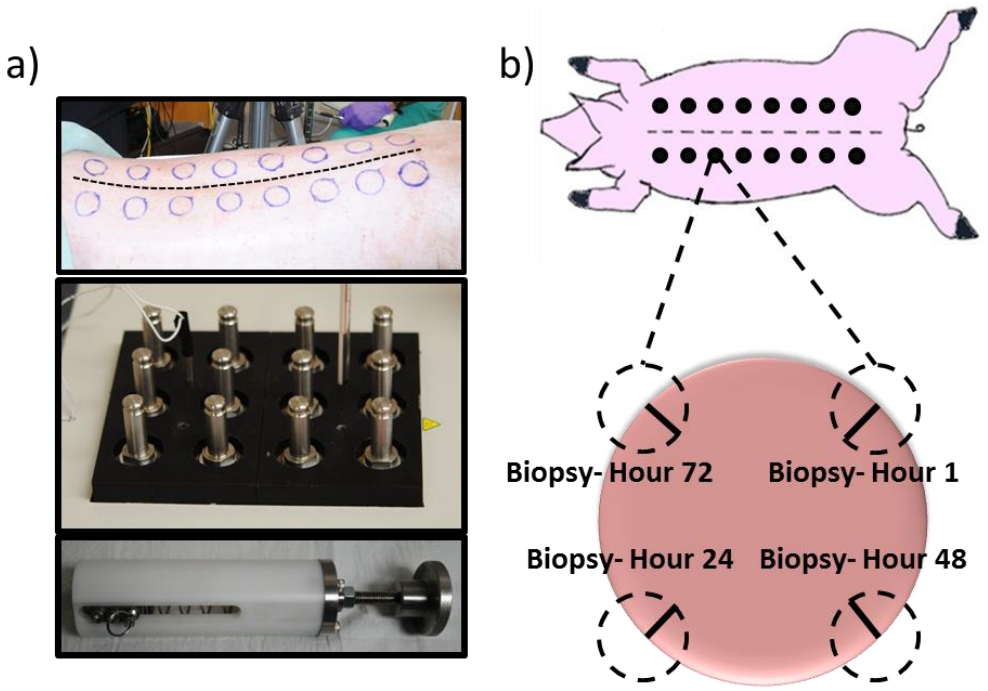

Fig. 2. Methodology of burn wound creation. a) Top panel shows the dorsum of a pig, with outline for wound spaces delineated. Serrated line shows the spine of the animal. Bottom panels show custom made device made to handle 3cm brass blocks. Spring-loaded device ensures consistent applied pressure. b) Cartoon schematic of the animal highlighting the 3 cm wounds created. For every wound, biopsies (dashed circles) were taken just after burn wound creation (hour 1) as well as hours 24, 48, and 72 post-burn. Solid black lines indicate approximate histological section.

2.5 Histopathology

After the creation of the burn areas at 1 hour post burn, and then again every subsequent day at approximately 24, 48 and 72 hours post-burn, 8 mm biopsy punches were taken from the edge of each burn wound for histological analysis (Fig. 2(b)). Skin biopsies were fixed in

#217716 - $15.00 USD Received 24 Jul 2014; accepted 28 Aug 2014; published 8 Sep 2014

10% buffered formalin for 48 hours, processed, embedded in paraffin and then cut into 6 μm cross-sectional slices. Slides were cleared in xylene and rehydrated to water where they were ready for staining. Masson's trichrome stain (Sigma Aldrich, Catalog HT-15) was performed for determination of burn severity.

Sections from entire wound biopsies were imaged at 4x magnification, and subsequently stitched together. Measurement of burn depth was performed with ImagePro software version 6.2 (Media Cybernetics, Bethesda, MD). For each biopsy image, the edge of the wound was identified as the disappearance of fibrillar collagen in the reticular layer of the dermis. The entire area from this edge through the rest of the biopsy (the burned portion of the biopsy) represented ~74% of the entire width of the biopsy. Burn depth (as defined by collagen coagulation) was measured at 5 evenly spaced intervals beginning with the edge of the wound bed, extending to the border of the biopsy (Fig. 3(b)). The five values were averaged to give an overall percentage of collagen coagulation (e.g. burn severity: superficial partial thickness, deep partial thickness, full thickness) for each wound on each day.

2.6 Statistical analysis

For each burn category (superficial partial thickness, deep partial thickness and full thickness burns), a series of paired student's t-tests were used to assess differences in stO_2 and scattering properties measured through SFDI, blood flow measured using LSI and collagen coagulation as reported by histology. In order to analyze each parameter deduced using LSI and SFDI image information, a region of interest (ROI) within the burn wound was selected. This ROI was within the burned section of the region that was biopsied after imaging (each day). Four control regions were also selected away from the burned areas to be used as normal tissue. The values of each parameter were averaged across burns of the same severity and are represented as box and whisker plots where the bottom and top of the boxes show the first and third quartiles, the band inside the box is the second quartile (the median), and the ends of the whiskers represent the min and max value. A p value less than 0.05 was considered statistically significant for this study.

3. Results

3.1 Histology measured collagen coagulation changes

Macroscopic color (Fig. 3(a)) and histology images (Fig. 3(b)) at 24 hours for representative burn wounds are shown. Partial thickness burns (both superficial and deep) appeared pale/blanched throughout the spatial extent of the wound. All burn wounds were delineated by a prominent red ring representing the zone of hyperemia [37]. Superficial partial thickness burns were indistinguishable from deep partial thickness burns based on visual inspection as both burns appeared pale/blanched (Fig. 3(a)). In contrast, full thickness burn wounds appeared leathery and darker, as has been described in the clinical literature [38] allowing for straightforward visual identification. Masson's trichrome staining (Fig. 3(b)) did, however, enable a distinction between superficial partial, deep partial, and full thickness burn wounds. The staining, commonly used to assess the depth of burn injury [39], results in connective tissue (i.e. collagen) appearing blue, muscle appearing dark red, and the epithelium a light pink/magenta. Highlighting the collagen makes it easier to visualize the damage and subsequent disorganization associated with collagen coagulation. Figure 3(b) shows solid lines marking the depth of collagen coagulation, while dashed lines show undamaged, structured collagen. Histological quantification of collagen coagulation [40] revealed a statistically significant correlation between probe contact time and burn severity as assessed by collagen coagulation at 24 hours post injury (Fig. 3(c)). This correlation ($r^2 = 0.84$) was better than what was seen immediately post-burn, however, there was not a progressive improvement in the correlation at hours 1, 48 and 72 ($r^2 = 0.72$, 0.89 and 0.78, respectively; data not shown).

#217716 - $15.00 USD Received 24 Jul 2014; accepted 28 Aug 2014; published 8 Sep 2014

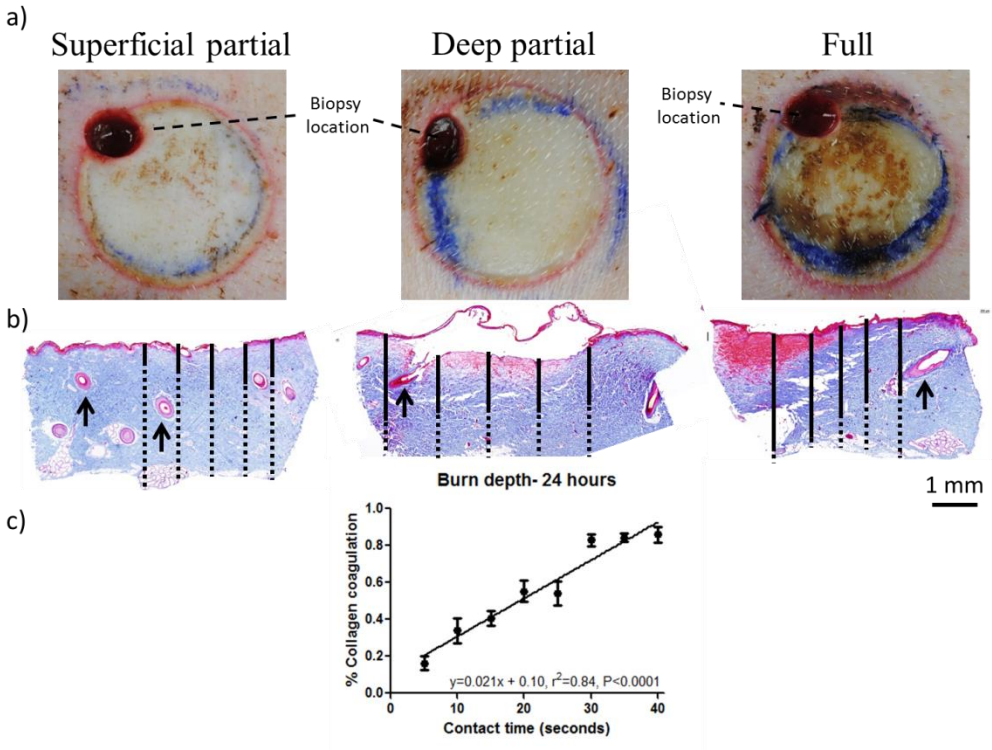

Fig. 3. a) Color images of representative burn regions at 24 hours. A prominent red ring representing the zone of hyperemia clearly delineates the edge of the wound bed and the initial 1 hour biopsy punch can be seen in the upper left corner of each wound. b) Trichrome images of burns 24 hours post-injury for 10 second (superficial-partial thickness), 20 second (deep partial thickness) and 40 second (full thickness) burns. Solid black lines indicate collagen coagulation depth, while dashed black lines indicate full thickness of the skin sample. Arrows indicate fully epithelialized hair follicles in superficial burns, while hair follicles in deep partial and full thickness burns are damaged with the epithelium sloughed off. c) Quantification of collagen coagulation depth reveals that contact time correlates well with percent dermal collagen coagulated as determined from histology at 24 hours post injury.

Examining the average collagen coagulation in histology for different burn contact time over the course of all four days further highlights the linear relationship between the two. By 24-hours post-injury it was possible to split burns into three distinct categories (Fig. 4). Contact times of 5 and 10 seconds were categorized as superficial partial thickness burns with typical values of collagen coagulation below 35%, while contact times of 30, 35 and 40 seconds were categorized as full thickness burns and showed over 65% collagen coagulation. Contact times of 15, 20 and 25 seconds were categorized as deep partial thickness burns and remained in between 35% and 65% coagulation. The difference in collagen coagulation for superficial and deep partial burns was statistically significant at hour 1 ($p<0.001$), 24 ($p<0.001$), 48 ($p<0.001$) and 72 ($p = 0.001$).

#217716 - $15.00 USD Received 24 Jul 2014; accepted 28 Aug 2014; published 8 Sep 2014

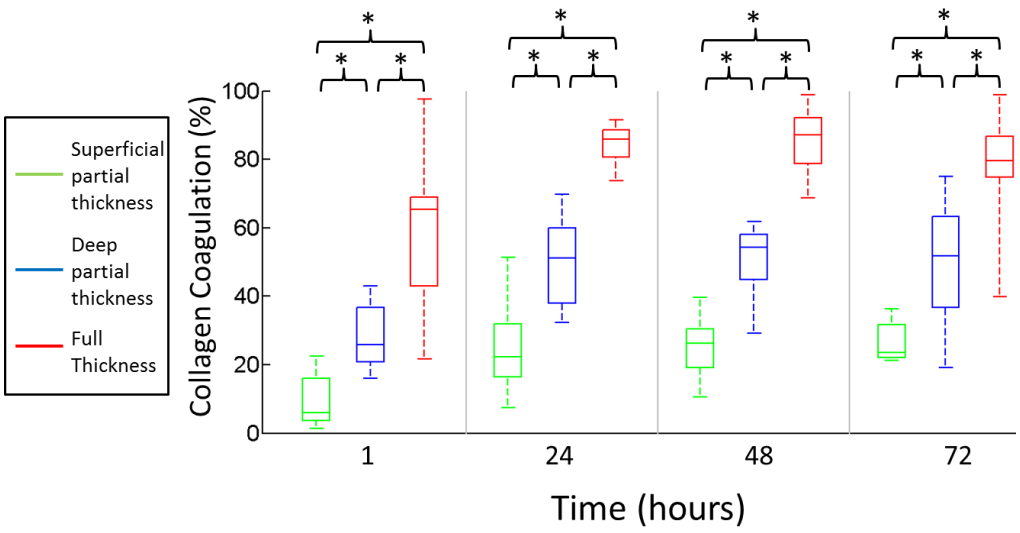

Fig. 4. Box and whisker plot of average collagen coagulation for three distinct burn categories. Time points at which there were statistically significant differences between groups are indicated with an asterisk.

3.2 LSI measured blood flow changes

Changes in blood flow measured using LSI and quantified through the speckle flow index are depicted in Fig. 5. An example of a typical LSI image for each burn category is shown on hour 1 and hour 72 (Fig. 5(a)). While all burn wounds experienced a decrease in blood flow from normal tissue (SFI of 923), more severe burns experienced a larger reduction in blood flow. The difference in blood flow for superficial partial thickness and deep partial thickness burns was statistically significant at hours 1 ($p = 0.002$), 24 ($p = 0.004$), and 72 ($p = 0.007$) (Fig. 5(b)). While there were statistically significant differences between superficial partial thickness and full thickness burns at all time points (hour 1 ($p<0.001$), hour 24 ($p = 0.003$), hour 48 ($p = 0.008$) and hour 72 ($p<0.001$)), there were no statistically significant differences in SFI between deep partial thickness and full thickness burns.

#217716 - $15.00 USD Received 24 Jul 2014; accepted 28 Aug 2014; published 8 Sep 2014

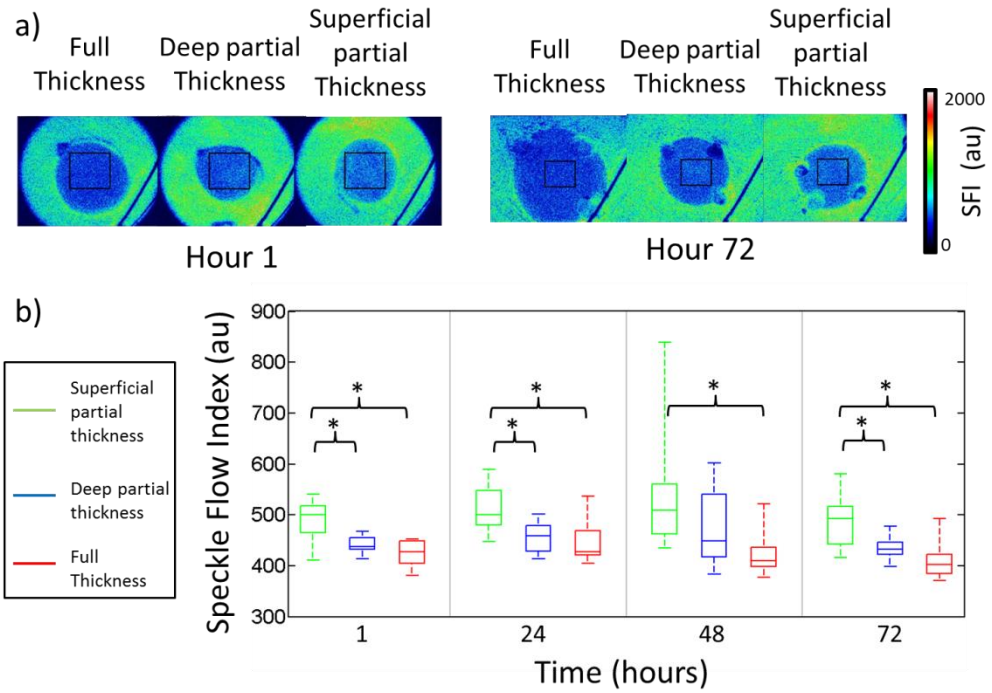

Fig. 5. a) Representative images of blood flow for the three burn categories at hour 1 and hour 72. b) Box and whisker plot of average blood flow for different burn categories as determined using laser speckle imaging. Time points with statistically significant differences between groups are indicated with an asterisk.

3.3 SFDI measured oxygen saturation changes

The SFDI derived stO_2 images for a typical superficial partial thickness burn and one of the more severe full thickness burns are shown in Fig. 6(a). A box and whisker plot of stO_2 values is shown in Fig. 6(b) below. While there was a decrease in stO_2 values from normal tissue oxygen saturation (64%) across all burn wounds, there were no statistically significant differences between the superficial partial thickness and deep partial thickness burn groups across any of the days observed. There were statistically significant differences in stO_2 between deep partial thickness and full thickness burn groups at hour 24 ($p = 0.006$) and hour 48 ($p = 0.006$). There were also statistically significant differences between superficial partial thickness and full thickness burns at all time points (hour 1 ($p = 0.018$), hour 24 ($p = 0.008$), hour 48 ($p<0.001$) and hour 72 ($p = 0.016$)). Other parameters such as oxygenated and deoxygenated hemoglobin that can be quantified using SFDI were examined but provided similar results (data not shown).

#217716 - $15.00 USD Received 24 Jul 2014; accepted 28 Aug 2014; published 8 Sep 2014

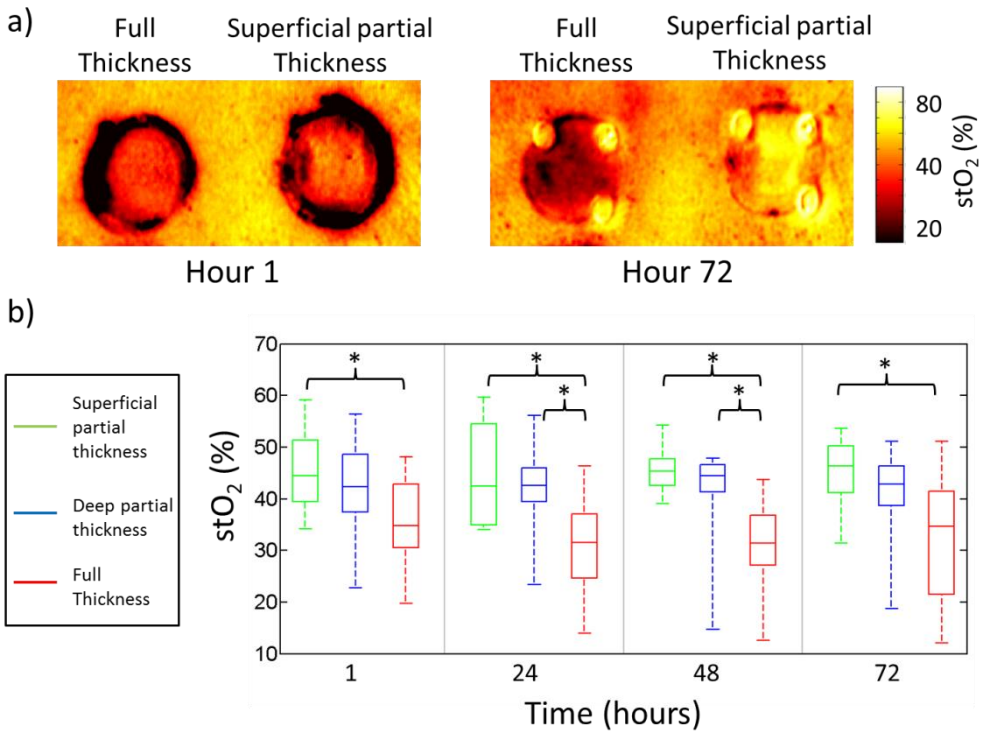

Fig. 6. a) Images of stO_2 for a superficial partial thickness burn and a full thickness burn at hour 1 and hour 72. b) Box and whisker plot of average stO_2 values for different burn categories. Time points with statistically significant differences between groups are indicated with an asterisk.

3.4 SFDI measured reduced scattering changes

Representative reduced scattering coefficient images (μ_s') at 850nm for the three different categories of burns are shown in Fig. 7(a) below. A box and whisker plot of the SFDI derived reduced scattering coefficient for all three burn categories is shown in Fig. 7(b). There was a decrease in the reduced scattering coefficient for full thickness burns relative to the reduced scattering coefficient for normal skin (1.12 mm^{-1}) as early as 1 hour after the burn. However partial thickness burns saw an increase in reduced scattering coefficient. There was a statistically significant difference in the reduced scattering coefficient for superficial partial thickness and deep partial thickness burns at hours 1 ($p = 0.002$), 24 ($p = 0.013$), 48 ($p = 0.010$) and 72 ($p = 0.008$) (Fig. 7(b)).

#217716 - $15.00 USD Received 24 Jul 2014; accepted 28 Aug 2014; published 8 Sep 2014

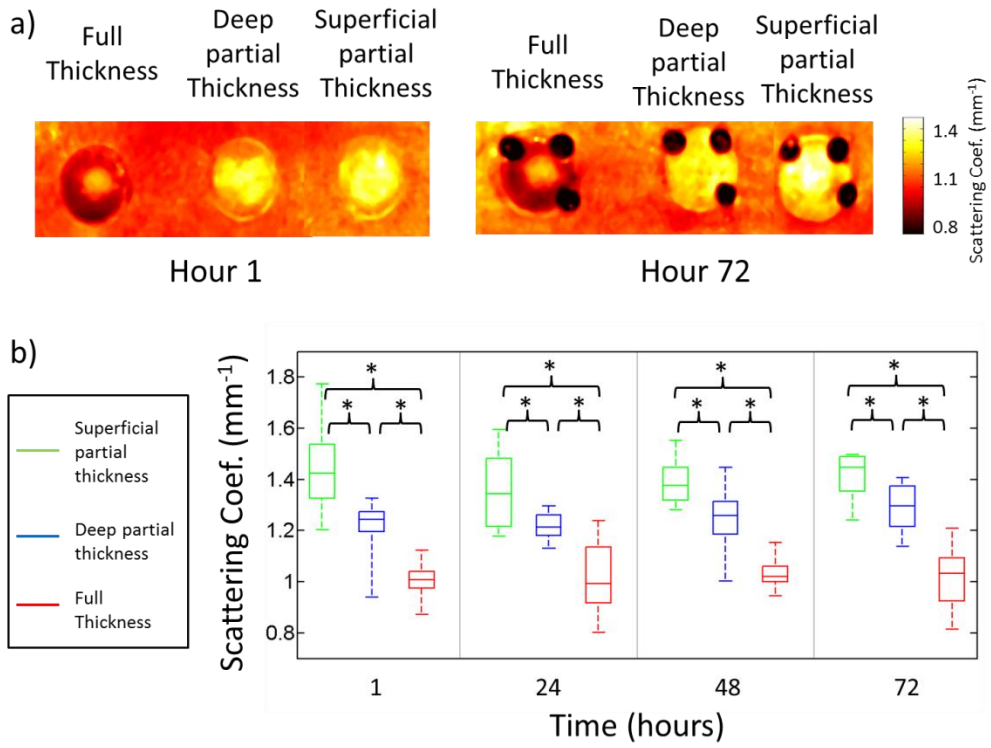

Fig. 7. a) Representative images of the reduced scattering coefficient for the three burn categories at hour 1 and hour 72. b) Box and whisker plot of average reduced scattering coefficient values for different burn categories. Time points with statistically significant differences between groups are shown with an asterisk.

3.5 Summary

Table 1 summarizes the average values obtained from the different methodologies at four distinct time points for superficial partial (SP), deep partial (DP) and full thickness (FT) burns.

Table 1. Summary of Results

	1 Hour			24 Hour			48 Hours			72 Hours		
Parameter	*SP*	*DP*	*FT*	*SP*	*DP*	*FT*	*SP*	*DP*	*FT*	*SP*	*DP*	*FT*
Collagen (%) Coagulation	9	28	59	25	50	84	25	51	85	26	51	78
Blood Flow (SFI)	490	441	426	512	456	445	542	472	425	487	434	411
stO_2 (%)	45	42	36	45	42	31	46	42	30	45	40	32
μ_s' (mm^{-1})	1.44	1.21	1.01	1.36	1.22	1.02	1.39	1.25	1.04	1.41	1.29	1.02

4. Discussion

While we have previously shown the ability to create controlled burn wounds in a rat model [28], porcine skin more closely resembles human skin in terms of optical and anatomic properties, including thickness [29]. Here we have demonstrated the ability to consistently create wounds of graded burn severity in a porcine model (Fig. 3(c)). By using collagen coagulation as reported by histological assessment of biopsies to verify burn extent, we were

#217716 - $15.00 USD Received 24 Jul 2014; accepted 28 Aug 2014; published 8 Sep 2014

able to reliably categorize burn wounds into superficial partial thickness, deep partial thickness and full thickness. One challenge of relying on histological assessments from punch biopsies is the potential for sampling variability from heterogeneous burns. Spatial heterogeneity in porcine models of thermal injury has been well documented before [29, 41–43], and despite focused efforts to create spatially homogeneous burn wounds, there is some expected heterogeneity in the current study. Still, the effect of contact time is the dominating factor for differences in burn depth among wounds. Moreover, the benefit of using imaging technologies having the inherent ability to provide spatially resolved information is that these techniques enable the user to select regions of interest in the image data that co-register with the biopsy area in order to make measurements on different days directly comparable.

The collection of biopsies tissue from burn regions is necessary to determine the true extent (depth) of injury [4]. For a longitudinal study over the course of several days, this introduces the potential that the biopsy wound could become a confounding factor when analyzing the burn wound. However, we have taken steps to mitigate this by placing the biopsies along the perimeter of the wound to maximize the distance between them and ensure only a small section of the burn wound is disturbed. Additionally, because we employed the same biopsy procedure on all burn wounds, the effects of this would be seen across all groups and not affect the ability of the techniques described to categorize the burn wounds.

While full thickness burns can typically be easily distinguished from partial thickness burns, superficial partial thickness and deep partial thickness burn initially look similar (Fig. 3(a)) and are typically not differentiated clinically until several days after the burn injury [2–4]. Because earlier intervention has been shown to shorten hospital stays [7–9] and improve the healing response for patients [6], we examined these burn wounds with LSI and SFDI shortly after the initial burn and for three days post-burn to determine when these imaging techniques could reliably categorize burn severity.

LDI has emerged as a popular technique for examining burn wounds [2, 5, 11] because of its ability to assess burns earlier and more accurately than a clinical assessment [5, 44]. However, studies have shown that LDI is not significantly better than clinical assessment until day 3 following a burn injury [5]. In this study we saw that LSI was able to detect decreases in blood flow that correlated with burn severity shortly after the burn wound was created. This flow information could be used to distinguish superficial partial thickness burns from deep partial thickness burns. However, this success is likely due to the controlled environment that these burns were created and in which our measurements were made. In a typical clinical environment, because of the variability from patient to patient and the dynamic nature of blood flow shortly after an injury, many groups have concluded that looking at changes in blood flow alone (using LDI or LSI) is generally not sufficient (less than 80% accurate) for categorizing partial thickness burn wounds during the initial 24 hours [2, 5, 44, 45]. The advantage of LSI is that it can quickly provide blood flow information non-invasively over a large field of view without the need to scan a laser source. The benefit of blood flow data has been suggested by literature that has reported on LDI results, however, this technology that reports flow does not provide insight into the important structural changes that occur in burn wounds shortly after injury.

As illustrated in the results, SFDI can be used to quantify chromophore concentrations and optical properties over a wide field-of-view. Observed changes in SFDI derived parameters such as the reduced scattering coefficient may be useful for rapidly and non-invasively assessing burn severity (Fig. 7). Changes in blood flow are a physiological response to a burn injury, but changes in scattering properties are a direct result of changes to the size and structure of the tissue as a result of the thermal damage. This is a likely reason we can see such dramatic changes in scattering properties one hour after the burn injury (Fig. 7(a)), similar to what we have seen previously in rats [28]. While the time to collect and analyze SFDI data (approximately one minute) is longer than is required for LSI, SFDI is capable of quantifying the structural information that could be useful for categorizing burn wounds

#217716 - $15.00 USD Received 24 Jul 2014; accepted 28 Aug 2014; published 8 Sep 2014

shortly after injury. SFDI is also capable of measuring physiological parameters including local tissue oxygen saturation, oxygenated hemoglobin and deoxygenated hemoglobin, but none were capable of reliably distinguishing burn categories over the four days we observed the wounds. We do expect that these parameters will have the potential for quantifying the dynamic healing response of burns typically seen about one week after the initial injury [45]. We expect that this capacity will be interesting within the context of looking at various burn wound healing interventions

One challenging aspect of making measurements in a clinical environment is the intrinsic variability in skin from patient to patient. A benefit of examining burn wounds is that the damage resulting from the burn process likely overwhelms this variability. Differences between individuals related to differences in pigmentation, skin hydration, and the changes in collagen associated with aging are likely overwhelmed by destruction of the epidermal layer where melanin resides, edema creating changes in water concentration, and the denaturation/hyalinization of collagen respectively. A unique facet of burn wound care in the United States is that more than 75% of the cases that require hospitalization are handled by one of the 127 hospital burn centers [5]. If the proposed work provides significant improvement over the current standard of care, it would be reasonable to get this technology into a large number of burn centers so that the benefits could be seen by the most patients. The information provided by SFDI and LSI also has the potential to be used for more than just burn wound categorization. By quantifying several aspects of tissue health, this technology has the ability to carry out quantitative longitudinal research oriented around assessment of the efficacy of different burn treatment options.

5. Conclusion

We have investigated two non-invasive tools: SFDI, capable of characterizing in-vivo scattering and absorption changes, and LSI, capable of characterizing blood flow changes, as methods to non-invasively predict burn severity. Burns ranging from superficial partial thickness to full thickness in a porcine model were monitored over three days. Here, we have demonstrated that monitoring changes in blood flow can distinguish superficial partial and deep partial thickness burns at one hour after burn injury. Additionally changes in the reduced scattering coefficient can differentiate superficial partial, deep partial and full thickness burns at one hour after injury. These techniques have the potential to predict burn severity at the earliest stages, which is critical for guiding treatment options.

Acknowledgments

We gratefully acknowledge support from the Beckman Foundation and the NIH, including P41EB015890 (A Biomedical Technology Resource), UL1 TR000148 and the Military Medical Photonics Program (AFOSR FA9550-10-1-0538). The content is solely the responsibility of the authors and does not necessarily represent the official views of the NIH.